

Factors governing the formation and persistence of layers in a subalpine snowpack

David Gustafsson,¹ Peter A. Waldner^{2*} and Manfred Stähli²

¹ Department of Land and Water Resources Engineering, Royal Institute of Technology, SE-100 44 Stockholm, Sweden

² Swiss Federal Research Institute WSL, Zürcherstrasse 111, CH-8903 Birmensdorf, Switzerland

Abstract:

The layered structure of a snowpack has a great effect on several important physical processes, such as water movement, reflection of solar radiation or avalanche release. Our aim was to investigate what factors are most important with respect to the formation and persistence of distinct layers in a subalpine environment. We used a physically based numerical one-dimensional model to simulate the development of a snowpack on a subalpine meadow in central Switzerland during one winter season (1998–99). A thorough model validation was based on extensive measurement data including meteorological and snow physical parameters. The model simulated the snow water equivalent and the depth of the snowpack as well as the energy balance accurately. The observed strong layering of the snowpack, however, was not reproduced satisfactorily. In a sensitivity analysis, we tested different model options and parameter settings significant for the formation of snow layers. The neglect of effects of snow microstructure on the compaction rate, and the current description of the water redistribution inside the snowpack, which disregard capillary barrier effects, preferential flow and lateral water flow, were the major limitations for a more realistic simulation of the snowpack layering. Copyright © 2004 John Wiley & Sons, Ltd.

KEY WORDS snowpack; layering; numerical simulation model; subalpine

INTRODUCTION

A snow cover is a complex composition of layers formed by numerous snowfall and melt events. This layered nature of the snow cover has special implications for some important physical processes such as avalanche release, adsorption and reflection of solar radiation, and meltwater movement. Avalanches are often triggered by weak snow layers in the snowpack, including buried surface-hoar. Hence, a precise prediction of the snowpack layering is vital for the avalanche risk assessment. Accurate simulation of the radiation balance in snow-covered areas is a key issue in meteorological modelling, as well as for an improved interpretation of remote sensing data, e.g. in the microwave range (Wiesmann and Mätzler, 1999). The extinction or reflection of solar radiation at the snow surface is often a complex process involving the very contrasting optical properties of adjacent snow layers, which makes it necessary to account for the snowpack layering. Meltwater movement in a snowpack is not at all a homogeneous one-dimensional flow, as we naively could expect. Owing to sharp boundaries between layers of fine and coarse grains capillary barriers arise, resulting in strong lateral water flow and a pronounced finger pattern (Marsh and Woo, 1984).

Recognizing the importance of the layered snowpack structure, snow modellers started to develop numerical multiple-layer snow models, including detailed process description of snow accumulation, metamorphism, melt, water and heat flow. During the past two decades several numerical models have been developed, tested and also successfully applied in operational forecast systems in the alpine regions of Europe and North

* Correspondence to: Peter A. Waldner, Swiss Federal Research Institute WSL, Zürcherstrasse 111, CH-8903 Birmensdorf, Switzerland. E-mail: peter.waldner@wsl.ch

America. The following are the three most prominent of these multiple-layer snow models: SNTHERM, CROCUS and SNOWPACK.

SNTHERM (Jordan, 1991) is an energy and mass balance model, developed at the US Army Corps of Engineers, Cold Regions Research and Engineering Laboratory. The main objective of the model is the prediction of snow temperature. However, densification processes as well as water and vapour transport are included in the model as parts of the heat balance.

CROCUS (Brun *et al.*, 1989, 1992), developed at the French Weather Service Météo-France, has become an operational tool for avalanche hazard assessment. A strength of the model is the detailed description of metamorphism processes for different types of snow, taking into account the size and shape of the snow grains.

SNOWPACK (Lehning *et al.*, 1999) is the snowpack model of the Swiss Federal Institute for Snow and Avalanche Research, Davos. Two special features of the model are (i) the simulation of snow precipitation, based on snow-depth measurements, and (ii) estimation of the density of new snow from the meteorological conditions.

These models have been calibrated and validated extensively at selected field sites (Brun *et al.*, 1992; Rowe *et al.*, 1995; Durand *et al.*, 1999; Jordan and Andreas, 1999; Lehning *et al.*, 1999; Koivusalo *et al.*, 2001). To our knowledge, however, only very few such tests have been published showing how successfully these models reproduce the layering of subalpine snowpacks that are subjected to frequent melting and refreezing throughout the winter season.

In the present article we intend to address this snow-cover type, which characterizes large parts of central Europe. We used the SNTHERM model (Jordan, 1991) incorporated into the soil–vegetation–atmosphere transfer model COUP (formerly SOIL, WINSOIL) (Jansson and Moon, 2001, <http://www.lwr.kth.se/coup.htm>) and in addition, the SNOWPACK model (Lehning *et al.*, 1999).

The overall goal was to test the ability of the SNTHERM model to simulate seasonal development of the snowpack layering at a subalpine site (1200 m a.s.l.) where air temperature shifts frequently between well below and above freezing point in a normal winter. Our objectives were (i) to determine the effect of the widely varying snow surface conditions on the formation and persistence of the snow layer pattern, (ii) to assess the capability of the model to explain the observations by sensitivity analysis of model parameters and options, and (iii) to identify relevant processes that are not included in the model.

MATERIALS AND METHOD

Model description

SNTHERM is a numerical model for the simulation of heat and mass in a one-dimensional snowpack based on a finite difference scheme. The accumulation and melt of the snowpack and its layers are determined entirely by the meteorological conditions that are put in the model in the form of continuous measurements of standard meteorological parameters (temperature, precipitation, wind speed, relative humidity and solar radiation or cloudiness).

In the present application, SNTHERM is incorporated, with some minor modifications (Gustafsson *et al.*, 2001), in the soil–vegetation–atmosphere transfer model COUP, which simulates the heat and water fluxes at the soil surface and in the layered soil profile. COUP optionally includes processes of water and radiation interception and evapotranspiration if a plant cover is present, or groundwater flow if a shallow groundwater table can be assumed. Both models have been described frequently in the literature (e.g. Johnsson and Jansson, 1991; Hardy *et al.*, 1998; Stähli *et al.*, 1999; Koivusalo *et al.*, 2001). In the following sections we will explain in detail those parts that are important with regard to the present application.

Density of new-fallen snow. The transition between rain and snow, which is a frequent situation in a subalpine environment, is a sensitive process owing to the rapid shift in the density and the latent heat of the

snow. When air temperature drops below a threshold temperature $T_{\text{Rain,Lim}}$ ($^{\circ}\text{C}$) precipitation turns from pure rain to snow. At temperatures below $T_{\text{Snow,Lim}}$ ($^{\circ}\text{C}$) all precipitation is assumed to fall as dry snow. The model has two options to calculate the density of new-fallen snow for air temperatures, T_{air} ($^{\circ}\text{C}$), below $T_{\text{Rain,Lim}}$

linear model:
$$\rho_{\text{snow,new}} = \rho_{\text{snow}^*} + 181 \text{ kg m}^{-3} \times f_{\text{liq}} \quad (1)$$

exponential model:
$$\rho_{\text{snow,new}} = \frac{\rho_{\text{snow}^*}}{\rho_{\text{HP}}(T_{\text{Snow,Lim}}) \times (1 - f_{\text{liq}})} \rho_{\text{HP}}(T_{\text{air}}) \quad (2)$$

Here ρ_{snow^*} (kg m^{-3}) is a parameter for the new snow density at $T_{\text{air}} = T_{\text{Snow,Lim}}$, $\rho_{\text{HP}}(T)$ is the density function of Hedstrom and Pomeroy (1998)

$$\rho_{\text{HP}} = 67.92 \text{ kg m}^{-3} + 51.25 \text{ kg m}^{-3} e^{(T/2.59)^{\circ}\text{C}} \quad (3)$$

and f_{liq} (kg kg^{-1}) the fraction of liquid water in mixed precipitation. The f_{liq} is given as (Jansson and Moon, 2001)

$$f_{\text{liq}} = f_{\text{liq,max}} \frac{T_{\text{Rain,Lim}} - T_{\text{air}}}{T_{\text{Rain,Lim}} - T_{\text{Snow,Lim}}} \quad (4)$$

with $f_{\text{liq,max}}$ (kg kg^{-1}) as the maximum fraction of liquid water in mixed precipitation.

Heat balance calculation. The heat balance for a snow layer is expressed as

$$-\frac{\partial(Tc)}{\partial t} = q_{\text{h,snow}} + q_{\text{h,melt}} + q_{\text{h,prec}} + H + LE - R_{\text{net}} \quad (5)$$

where $-\partial Tc/\partial t$ (T is temperature, c is heat capacity) is the net heat change, which is balanced by R_{net} , the net absorption of shortwave and longwave radiation, H , the sensible heat flux to the atmosphere, LE , the latent heat flux to the atmosphere, $q_{\text{h,melt}}$, the snowmelt energy, $q_{\text{h,prec}}$, the heat flux with precipitation and $q_{\text{h,snow}}$, the net heat flux for each layer, including heat flux with liquid water flow and water vapour flow. All units are W m^{-2} . Equation (5) is solved for each layer, with the exception of H , LE and $q_{\text{h,prec}}$, which are included only for the surface layer.

The R_{net} above the snow surface is calculated as

$$R_{\text{net}} = R_{\text{S}\downarrow}(1 - \alpha_{\text{snow}}) + R_{\text{L}\downarrow} - \sigma(T_{\text{S}} + 273.15)^4 \quad (6)$$

where $R_{\text{S}\downarrow}$ (W m^{-2}) is the measured incoming shortwave radiation, α_{snow} (–) the snow surface albedo, $R_{\text{L}\downarrow}$ (W m^{-2}) the measured or simulated incoming longwave radiation and T_{S} ($^{\circ}\text{C}$) the snow surface temperature.

If measurements of $R_{\text{L}\downarrow}$ are missing, the formula of Konzelmann *et al.* (1994) is used

$$R_{\text{L}\downarrow} = \left\{ \left(r_{\text{k1}} + r_{\text{k2}} \left[\frac{e_{\text{air}}}{T_{\text{air}} + 273.15} \right]^{1/8} \right) (1 - f_{\text{cloud}}^3) + r_{\text{k3}} f_{\text{cloud}}^3 \right\} \sigma(T_{\text{air}} + 273.15)^4 \quad (7)$$

where f_{cloud} (–) is cloudiness and e_{air} (Pa) is air vapour pressure, with the three parameters r_{k1} (–), r_{k2} ($\text{K Pa}^{-1/8}$) and r_{k3} (–). The cloudiness is estimated from measured incoming shortwave radiation and potential global radiation, using the formula of Ångström (1924). For the albedo, α_{snow} , of the snow surface an equation based on the ideas of Plüss and Mazzoni (1994) is applied

$$\alpha_{\text{snow}} = \alpha_{\text{min}} + a_1 e^{(a_2 S_{\text{age}} + a_3 \sum T_{\text{air}}^+)} \quad (8)$$

where α_{min} (–) is the minimum snow albedo, S_{age} (day) is the number of days since the last snowfall, $\sum T_{\text{air}}^+$ ($^{\circ}\text{C day}$) is the sum of daily positive air temperatures since the last snowfall, and a_1 (–), a_2 (day^{-1}) and a_3 ($^{\circ}\text{C}^{-1} \text{ day}^{-1}$) are parameters.

Absorption of shortwave radiation by snow is assumed to be proportional to the density. The penetration of $R_{S\downarrow}$ follows an exponential function from the surface down to 30 mm equivalent water depth. Longwave radiation is absorbed in the top layer only.

Snow settling. The compaction of a snow layer is expressed according to Jordan (1991) with three additive rate terms: (i) destructive metamorphism, (ii) overburden pressure and (iii) snowmelt

$$CR = -\frac{1}{\Delta z} \frac{\partial \Delta z}{\partial t} = CR_{\text{metam}} + CR_{\text{overburden}} + CR_{\text{melt}} \quad (9)$$

where CR is the compaction rate (s^{-1}) and Δz (m) is the layer thickness.

The compaction term CR_{metam} is described as a function of snow temperature, T_{snow} ($^{\circ}\text{C}$), bulk density of ice, γ_{ice} (kg m^{-3}), and bulk density of liquid water, γ_{liq} (kg m^{-3})

$$CR_{\text{metam}} = CR_{\text{Temperature}} \times CR_{\text{Density}} \times CR_{\text{Liquid}} \quad (10)$$

where

$$\begin{aligned} CR_{\text{Temperature}} &= c_1 \times e^{c_2 \times T_{\text{snow}}} \\ CR_{\text{Density}} &= e^{-c_3 \times \max[0, (\gamma_{\text{ice}} - \gamma_{\text{lim}})]}, \quad \gamma_{\text{lim}} = \min(\gamma_{\text{lim, max}}, 1.15 \times \gamma_{\text{ice, new}}) \\ CR_{\text{Liquid}} &= \begin{cases} 1 & \gamma_{\text{liq}} = 0 \\ c_4 & \gamma_{\text{liq}} > 0 \end{cases} \end{aligned} \quad (11)$$

with the parameters c_1 (s^{-1}), c_2 ($^{\circ}\text{C}^{-1}$), c_3 ($\text{m}^3 \text{kg}^{-1}$) and c_4 ($-$), and a threshold density, γ_{lim} (kg m^{-3}), taken as the minimum of $\gamma_{\text{lim, max}}$ (kg m^{-3}), and the bulk density of ice in new-fallen snow, $\gamma_{\text{ice, new}}$ (kg m^{-3}).

The compaction term $CR_{\text{overburden}}$ is calculated with

$$CR_{\text{overburden}} = \frac{P_s}{\eta_0} \times e^{(c_5 \times T_{\text{snow}} - c_6 \times \gamma_{\text{ice}})} \quad (12)$$

where P_s (kg m^{-2}) is the overburden pressure, η_0 (kg s m^{-2}) is a parameter representing viscosity at 0°C and $P_s = 0 \text{ kg m}^{-2}$, and c_5 ($^{\circ}\text{C}^{-1}$) and c_6 ($\text{m}^3 \text{kg}^{-1}$) are parameters representing the temperature and density influence on the compaction rate.

Finally, the compaction term CR_{melt} is given as

$$CR_{\text{melt}} = \frac{q_{\text{melt}}}{\gamma_{\text{ice}} \times \Delta z} \quad (13)$$

where q_{melt} ($\text{kg m}^{-2} \text{s}^{-1}$) corresponds to the rate of melt in the layer.

The modelled vertical snow profile is represented by finite, homogeneous layers. To prevent numerical instability the thickness of snow layers is restricted to a range between $z_{\text{sl, max}}$ (m) and $z_{\text{sl, min}}$ (m). If owing to compaction a snow layer decreases below $z_{\text{sl, min}}$ (m), it is merged with the thinnest neighbouring snow layer. Alternatively, in the case of a snow layer exceeding $z_{\text{sl, max}}$ (m), it will be split up into two layers.

Grain-size development. Snow grain size, d_{gr} (m), is the only property describing the microstructure of the snow. Snow grain growth, $\partial d_{\text{gr}} / \partial t$ (m s^{-1}), is calculated as an empirical function of water vapour flux q_v ($\text{kg m}^{-2} \text{s}^{-1}$) and of liquid water content for dry and wet snow, respectively (Jordan, 1991)

$$\frac{\partial d_{\text{gr}}}{\partial t} = \begin{cases} \frac{g_1 \times \max[|q_v|, q_{v, \text{max, gr}}]}{d_{\text{gr}}} & \theta_{\text{liq}} < \theta_{\text{liq, max, gr}} \\ \frac{g_2 \times (\max[\theta_{\text{liq}}, 0.09] + 0.05)}{d_{\text{gr}}} & \theta_{\text{liq}} \geq \theta_{\text{liq, max, gr}} \end{cases} \quad (14)$$

where g_1 ($\text{m}^4 \text{kg}^{-1}$) and g_2 ($\text{m}^2 \text{s}^{-1}$) are two rate parameters, and $q_{v,\text{max,gr}}$ ($\text{kg m}^{-2} \text{s}^{-1}$) and $\theta_{\text{liq,max,gr}}$ ($\text{m}^3 \text{m}^{-3}$) the upper limits of vapour flow and liquid water content. The grain size is not allowed to exceed 0.005 m.

The bulk density of ice in the precipitation, γ_{ice} (kg m^{-3}), determines the grain size of new-fallen snow, $d_{\text{gr,new}}$ (m)

$$d_{\text{gr,new}} = \begin{cases} 1.6 \times 10^{-4} + 1.1 \times 10^{-13} \times \gamma_{\text{ice}}^4 & \gamma_{\text{ice}} < 400 \\ 2.976 \times 10^{-3} & \gamma_{\text{ice}} \geq 400 \end{cases} \quad (15)$$

Water and vapour flow in the snowpack. Water redistribution between snow layers is calculated based on the gravity flow algorithm of Colbeck (1971). The mass flux of liquid water, q_{liq} ($\text{kg m}^{-2} \text{s}^{-1}$) is given as

$$q_{\text{liq}} = -\frac{K_{\text{liq}}}{\mu_{\text{liq}}} \rho_{\text{liq}}^2 g \quad (16)$$

where μ_{liq} ($1.787 \times 10^{-3} \text{ N s m}^{-2}$) is the dynamic viscosity of water, ρ_{liq} ($1 \times 10^3 \text{ kg m}^{-3}$) is the density of liquid water, g (9.81 m s^{-2}) is the acceleration of gravity, and K_{liq} (m^2) is the hydraulic permeability expressed in terms of the effective liquid saturation, s_e ($\text{m}^3 \text{m}^{-3}$),

$$K_{\text{liq}} = K_{\text{sat}} s_e^\varepsilon, \quad (17)$$

where ε (–) is a grain size distribution index. The effective liquid saturation is estimated from the residual liquid water saturation, $s_r = 0.04 \text{ m}^3 \text{m}^{-3}$

$$s_e = \frac{s - s_r}{1 - s_r} \quad (s = \theta_{\text{liq}}/\theta_{\text{porosity}}) \quad (18)$$

The permeability at full saturation, K_{sat} (m^2) is given as (Shimizu, 1970)

$$K_{\text{sat}} = k_{s1} d_{\text{gr}}^2 e^{(-k_{s2} \gamma_{\text{ice}})} \quad (19)$$

where d_{gr} (m) is the snow grain size, γ_{ice} (kg m^{-3}) is the bulk density of ice and k_{s1} (–) and k_{s2} ($\text{m}^3 \text{kg}^{-1}$) are empirical parameters.

Water vapour flow is calculated as (Jordan, 1991)

$$q_v = -D_{e,\text{snow}} C_{j,T_{\text{snow}}} \frac{\partial T_{\text{snow}}}{\partial z} \quad (20)$$

where $D_{e,\text{snow}}$ ($\text{m}^2 \text{s}^{-1}$) is the effective diffusion coefficient for snow, and $C_{j,T_{\text{snow}}}$ ($\text{N m}^{-2} \text{°C}^{-1}$) is the variation of the saturation vapour pressure with temperature relative to ice ($\theta_{\text{liq}} \leq 0.02 \text{ m}^3 \text{m}^{-3}$) or liquid water ($\theta_{\text{liq}} > 0.02 \text{ m}^3 \text{m}^{-3}$). The effective diffusion coefficient is given as

$$D_{e,\text{snow}} = D_{e0,\text{snow}} \left(\frac{1000}{P_a} \right) \left(\frac{T_{\text{snow}} + 273.15}{273.15} \right)^6 \quad (21)$$

where $D_{e0,\text{snow}} = 0.0009 \text{ m}^2 \text{s}^{-1}$ is the effective diffusion coefficient at 1000 hPa and 0 °C.

Site description and measurements

The measurements used for the model validation were carried out at Erlenhöhe in the valley of Alptal (central Switzerland; latitude 47 °N), a marshy meadow at an altitude of 1200 m a.s.l. The terrain slopes moderately (10–15% inclination) towards the west, and is fairly well protected from the wind by coniferous forest surrounding the measurement field at a distance of 50–150 m. A meteorological station collecting all standard climate variables is located at the site (Keller and Forster, 1991).

Complementary to these meteorological records, radiation components $R_{S\downarrow}$, $R_{S\uparrow}$, $R_{L\downarrow}$ and $R_{L\uparrow}$ were measured during parts of the experimental winter 1998/99 (January to April) using a CNR 1 radiometer (Kipp and Zonen Inc., Delft, The Netherlands). We calculated daily mean values of the albedo from the shortwave radiation measurements around noon (0900 to 1500 hours). Such daily mean values were best suited to be compared with simulated albedo because the model does not account for the within-day variation of albedo.

The snow survey during winter 1998–99, described in detail by Waldner *et al.* (2000), included the following measurements: snow depth was recorded continuously with an ultrasonic snow depth sensor (starting in mid-January), as well as manually every 3–10 days along a 30 m snow course (entire winter season). Average snow density and snow water equivalent (SWE) of the total snowpack were determined gravimetrically every 3–10 days using a tube of 7 cm diameter.

To photograph the true snowpack layering, translucent snow profiles were constructed on eight dates during the winter: snow pits were excavated from two sides exhibiting a 5-cm-thick and about 1-m-wide vertical cross-section of the original snow cover perpendicular to the sunlight using a long aluminum snow saw. The pit on the unilluminated side was covered with a black blanket to provide optimal light conditions for photographing the translucent snow monolith. Two polystyrene plates were used as references for light absorbance (grey scale), and height markers were punched at the edges of the profile. For the same dates a detailed determination of the snow density and grain-size profile was carried out using the terms of the international snow classification (Colbeck *et al.*, 1990). These properties were determined for layers of varying thickness subdivided according to our visual judgment.

Model inputs and parameter setting

The model was run for the period 10 November 1998 to 30 May 1999 with hourly inputs of air temperature, wind speed, relative humidity, precipitation, global radiation and—when available—incoming longwave radiation (January–April). A summary of the parameter settings is given in Table I. The parameters in the snow albedo function (Equation 8) were fitted to best reproduce the measured albedo in March and April, and yielded the following values: $\alpha_{\min} = 0.55$, $a_1 = 0.35$, $a_2 = -0.15 \text{ day}^{-1}$ and $a_3 = -0.05 \text{ }^\circ\text{C}^{-1} \text{ day}^{-1}$. The function for incoming longwave radiation (Equation 7) was parameterized according to Konzelmann *et al.* (1994) and the estimated $R_{L\downarrow}$ correlated reasonably well to the measurement (January–April: $R^2 = 0.59$).

Table I. Parameter values used in the default simulation

Parameter	Equation	Value	Parameter	Equation	Value
$f_{\text{liq,max}}$ (kg kg ⁻¹)	1, 2, 4	0.5	$\gamma_{\text{lim,max}}$ (kg m ⁻³)	11	100
ρ_{snow}^* (kg m ⁻³)	1, 2	110	c_5 (°C ⁻¹)	12	0.04
$T_{\text{Rain,Lim}}$ (°C)	4	2	c_6 (m ³ kg ⁻¹)	12	0.023
$T_{\text{Snow,Lim}}$ (°C)	4	0	η_0 (kg s m ⁻²)	12	9×10^5
r_{k1} (—)	7	0.23	g_1 (m ⁴ kg ⁻¹)	14	5×10^{-7}
r_{k2} (K ^{1/8} Pa ^{-1/8})	7	0.483	g_2 (m ² s ⁻¹)	14	4×10^{-12}
r_{k3} (—)	7	0.963	S_r (m ³ m ⁻³)	17	4
α_{\min} (—)	8	0.55	k_{s1} (—)	19	0.077
a_1 (—)	8	0.35	k_{s2} (m ³ kg ⁻¹)	19	0.0078
a_2 (day ⁻¹)	8	-0.15	$\theta_{\text{liq,max,gr}}$ (m ³ m ⁻³)	14	0.09
a_3 (°C ⁻¹ day ⁻¹)	8	-0.05	$z_{\text{sl,max,top}}$ (m)		0.018
c_1 (s ⁻¹)	11	2.77×10^{-6}	$z_{\text{sl,max,second}}$ (m)		0.033
c_2 (°C ⁻¹)	11	0.04	$z_{\text{sl,max,general}}$ (m)		0.08
c_3 (m ³ kg ⁻¹)	11	0.046	$z_{\text{sl,min}}$ (m)		0.005
c_4 (—)	11	2			

With regard to the turbulent fluxes above the snow cover, we applied a Richardson number stability correction and used a roughness length for momentum of 0.01 m and a roughness length for heat of 0.001 m (Gustafsson *et al.*, 2001).

The density of new-fallen snow at 0°C, ρ_{snow^*} , was set to 110 kg m⁻³, which is a rather high value compared with other studies, but reasonable for these subalpine conditions. The maximum fraction of liquid water in mixed precipitation was assumed to be 0.5. The maximum thickness, $z_{\text{sl,max}}$, of the uppermost layer was set to 0.018 m, of the second layer to 0.033 m and of all other layers to 0.08 m, whereas the minimum thickness, $z_{\text{sl,min}}$, was set to 0.005 m. Parameters related to settling (Equations 11 and 12), grain growth (Equation 14) and water redistribution (Equation 19) were set as suggested by Jordan (1991, 1996). A basic parameterization of the soil and site properties was taken from Stähli *et al.* (2000).

RESULTS

Winter 1998–99 was snow-rich in the central Swiss Alps. At Erlenhöhe the snow depth reached a maximum of 1.8 m (corresponding to a SWE of about 550 mm) in late February (Figure 1), which is more than usual for this location. The winter started with an early onset of snow accumulation (10 November), followed by a settling phase around Christmas and New Year. Typically for that altitude, the air temperature shifted frequently between above and well below zero during these months with an average of -2.0°C in November, -1.0°C in December and -0.1°C in January. In February, heavy snowfall set in, and a total amount of 600 mm of snow and rain precipitation was measured during this coldest month of the winter (average temperature -4°C). Afterwards, the severe winter weather continued with a number of additional snowfall events delaying the final snowmelt to the second half of April. However, once the snowmelt set in the snowpack disappeared rapidly.

The mean snow density of the snowpack increased gradually from somewhat less than 200 kg m⁻³ in November to about 450 kg m⁻³ during the snowmelt (Figure 2). A characteristic layering of the snowpack developed with layers of thickness varying from 1–2 cm to a maximum of 20–30 cm, visible in the translucent profiles and the snow density profile measurements of Figure 6. We observed differences in snow density between adjacent layers of more than 100 kg m⁻³ (see profile of 13 February in Figure 6). The density contrast between snow layers decreased towards the end of the winter season, and a profile with a more or less homogeneous density structure formed (see density profile of 29 April in Figure 6).

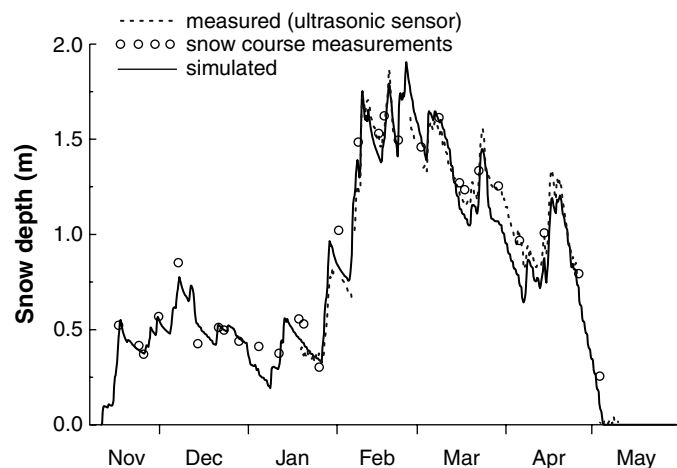


Figure 1. Simulated and measured snow depth at the Erlenhöhe site during winter 1998–99

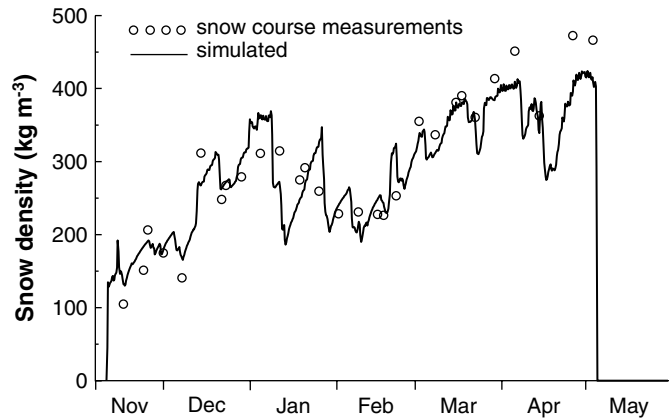


Figure 2. Simulated and measured bulk snow density at the Erlenhöhe site during winter 1998–99

In general, the model was able to accurately reproduce the development of the bulk properties of the snowpack, i.e. its depth and water equivalent. An excellent correspondence was achieved for simulated and measured snow depth compared with both the snow course measurements and the automatic ultrasonic sensor (Figure 1).

Also, the average density of the simulated snowpack agreed very well with the measurements (Figure 2). The well-predicted snow accumulation at the beginning of the winter indicated that the precipitation inputs to the model were trustworthy and the approach to estimate the new-snow density (Equation 2) was suitable to the conditions at Erlenhöhe. The time for short-term settling after snowfall events and the final ablation of the snowpack was simulated accurately, which led us to conclude that these two functions and the surface energy balance were reasonably well parameterized.

The reliability of the simulated snow surface energy balance was supported by the albedo (Figure 3) and net radiation measurements (Figure 4). The model simulated well the temporal variation of the albedo caused by fresh snow, snow surface ageing and melt, which ranged from minimum values of 0.55 to maximum values of 0.9. For cloudless days in mid-March, when the snowpack was more than 1 m thick, the net radiation

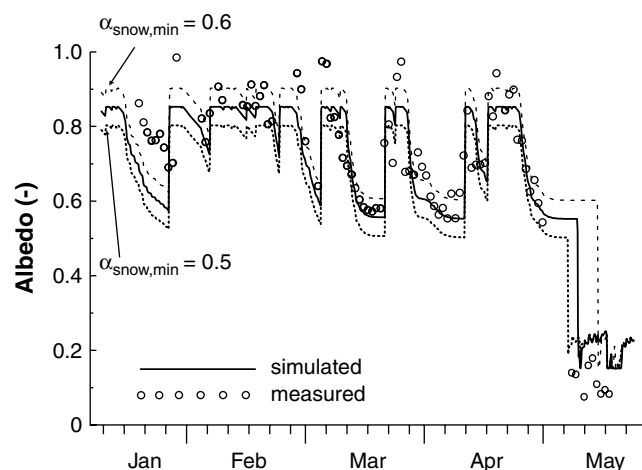


Figure 3. Simulated and measured albedo from January to May 1999. In addition to the default simulation, two simulations with increased and decreased albedo, respectively

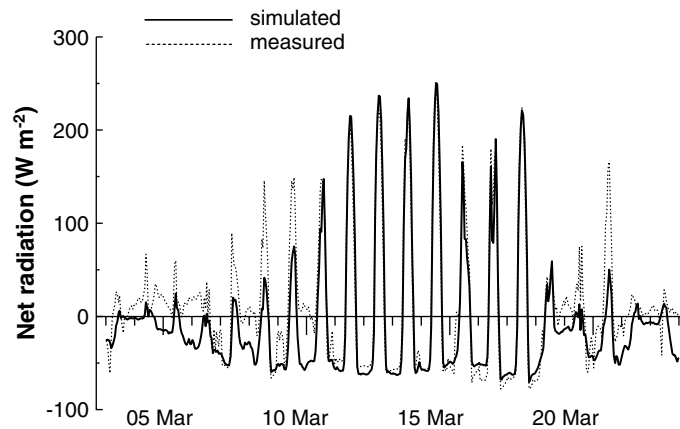


Figure 4. Simulated and measured net radiation for the period 4–23 March 1999

balance was very well reproduced by the model, especially with regard to the maximum irradiation at midday. However, for cloudy days, when the atmospheric longwave radiation was of major importance, the match between simulation and measurements was less favourable (e.g. 5–10 March).

The model realistically reproduced the natural compaction of the bulk snowpack in the course of the winter (Figure 2). Accumulation peaks of single snowfall events decreased within a few days, reflecting destructive metamorphism from fresh snow crystals toward rounded grains. Also the seasonal increase of the average snow density from about 200 kg m^{-3} to more than 400 kg m^{-3} was correctly produced with the model simulation (Figure 2). Layers with a higher density formed and persisted (e.g. in early February), primarily as a result of diurnal surface melt/refreeze cycles and subsurface refreeze of infiltrating meltwater. An illustrative example of dense snow layers forming owing to such short-term thawing and refreezing is given in Figure 5.

A closer look at the snow density profiles for single dates (Figure 6), however, shows that although the model reproduced well the general seasonal trend of the snowpack settling, it was less successful in reproducing the observed layers. In contrast to the real snowpack, where distinct differences between adjacent layers and pronounced boundaries between layers were observed, the simulated snow density varied only smoothly with depth. Distinct dense layers, such as the one at 60 cm above the soil surface on 13 February (see also Figure 6) were simulated only very weakly, and others, such as the layer at 80 cm above the soil surface on 2 March were missing altogether. Furthermore, the translucent profiles in Figure 6 tell us that the transition from one layer to another was more stepwise than continuous. The light transmission through snow profiles depends on the snow density and on the size and shape of snow grains and liquid water droplets (Bohren and Barkström, 1974). The light transmission profile shown in Figure 6 exhibits a distinct layering, which was not reproduced by the model, either during the accumulation or at the end of the season.

The lack of distinct layering with respect to the density goes hand in hand with a lack of a layered structure of the grain size. Our visual snowpack classifications showed that the grain size varied by up to 2 mm from layer to layer. For example on 10 March 1999 (Figure 7), we observed two distinct layers of small snow grain diameters in the lowest 40 cm of the profile (at $z = 0.21$ to 0.35 m and $z = 0.8$ to 0.9 m) alternating with thin layers of large grain size (e.g. at $z = 0.18$ to 0.21 m). The model simulation showed much less contrast in the vertical grain-size profile.

To summarize the comparison between observed and simulated snowpack, it can be stated that an excellent correspondence was achieved with respect to the general development of the depth, average density, surface radiation balance and temperatures (not shown in a graph). On the other hand, the contrasts in density and grain size between adjacent layers were not simulated satisfactorily by the model.

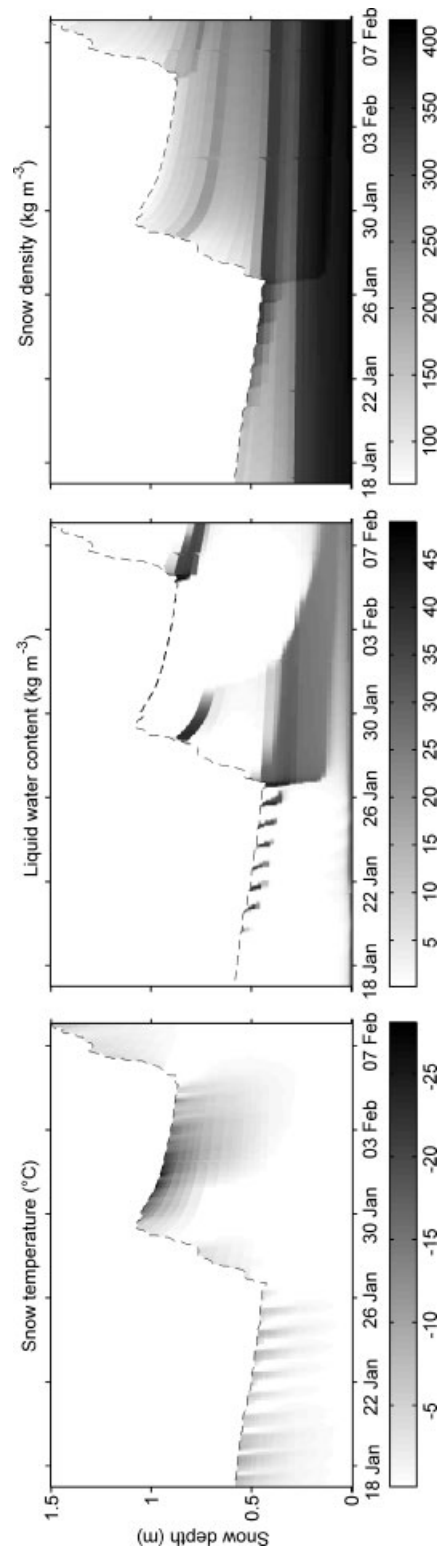


Figure 5. Simulated snow temperature (left), liquid water content (centre) and density (right) during and after some surface-melt/refreeze events, 17 January to 7 February 1999

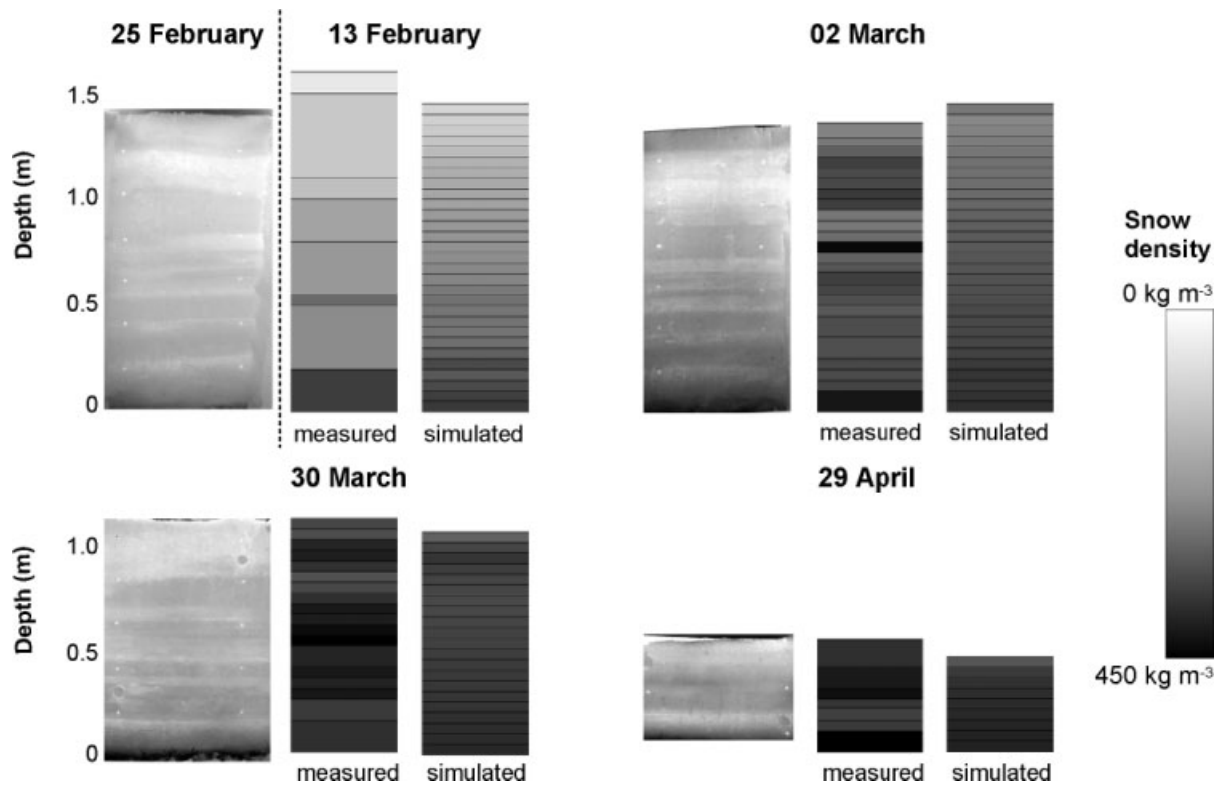


Figure 6. Translucent snow profiles (left), measured (centre) and simulated (right) snow density profiles for four stages of winter 1998–99. The grey colour bar indicates the values of the density profiles (linear scale)

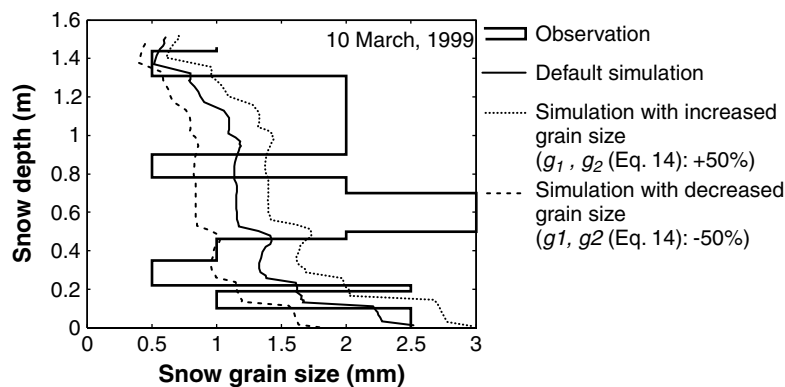


Figure 7. Observed and simulated depth profile of the snow grain size (mm) for 10 March 1999 at the Erlenhöhe site

Consequently, we focused on exploring (i) why this layer structure is smoothed out in the simulation, (ii) how we have to modify our model parameterization to achieve a more realistic snow layering, and (iii) which important processes dominating the formation and persistence of distinct layers are not adequately included in the model for this subalpine snowpack.

Sensitivity analysis

To identify the key processes forming and preserving distinct layers in a snowpack we made a sensitivity analysis based on the parameter setting in Table I. We varied single parameter values and model options, which we assumed had a major influence on the snow layer pattern.

Density of new-fallen snow. At Erlenhöhe where snow often falls at air temperatures close to 0°C a correct simulation of the density of new-fallen snow was assumed to be vital for the snow density profile and, as expected, simulated snow depth and densities were sensitive on $T_{\text{Rain,Lim}}$, $T_{\text{Snow,Lim}}$ and ρ_{snow^*} (not shown in a graph). When we compared the two formulations of the new-snow density (Equations 1 and 2) we noted slightly different snow depths during and shortly after major snowfall events (Figure 8). At most, the deviation in snow depth between the two approaches was 20 cm for the main snow accumulation period in winter 1999. However, during the following snow settling phase the two simulation curves grew closer together again owing to different compaction rates. Factors other than air temperature are also known to influence new snow properties, such as wind speed especially (Jordan and Andreas, 1999; Lehning *et al.*, 2002a,b), but wind remained rather weak at the specific site.

Surface energy balance. The surface energy balance, which governs melting, refreezing and metamorphism at the snow surface, is without any doubt an important factor for the formation of high-density layers or surface hoar. Thus, we hypothesized that both the radiation balance and the turbulent heat fluxes would be sensitive processes with respect to the snow layer development. In a first test, the snow albedo was increased and decreased, respectively, by 0.05 (Figure 4). This was achieved by changing the value of α_{min} in Equation 8. From that simulation resulted, of course, restricted or enhanced snow melting and, as a consequence, a thicker or thinner snowpack. With regard to the snow layering, a change of the albedo was not able to enhance the contrasts in snow density between adjacent layers more than marginally, neither did new distinct layers form (Figure 9).

We also changed the turbulent heat fluxes by increasing and decreasing the roughness length of momentum (z_{0m}), which has a default value of 0.01 m, to 0.02 m and 0.005 m, respectively. Also here, the effect on the

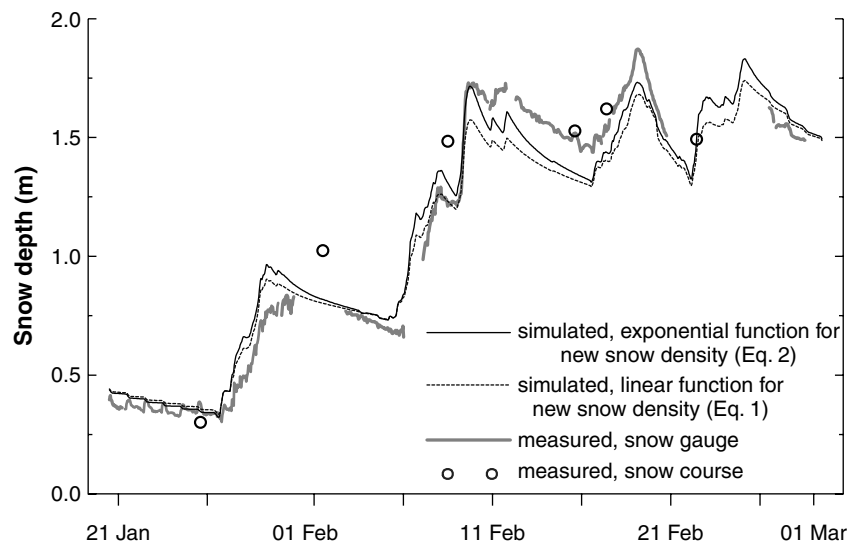


Figure 8. Test of two formulations determining the density of new-fallen snow (Equations 1 and 2): simulated and observed snow depth, 20 January to 1 March 1999

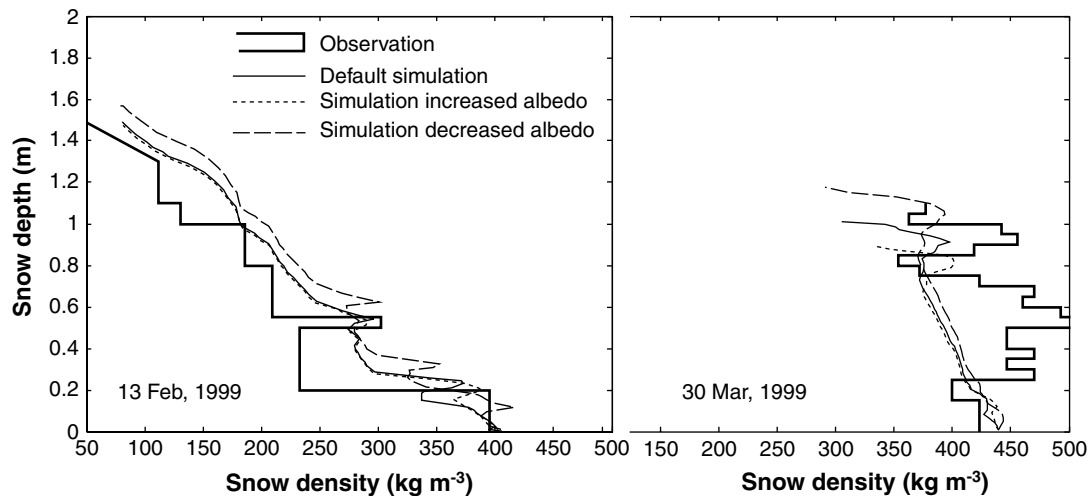


Figure 9. Sensitivity test of the snow albedo: simulated and observed snow density profiles for two dates in winter 1998–99

melt rates and the snow depth was considerable. With respect to the snow layering, however, a modified z_{0m} did not intensify the contrasts in snow density between adjacent layers.

To sum up, we conclude that increased or decreased snowmelt rates were not able to improve the simulated snow density profile. In view of the excellent agreement between measured and simulated net radiation and albedo achieved with the parameter values listed in Table I and the low sensitivity of the roughness length, we state that in the case of our subalpine snowpack the model parts related to the surface energy balance are *not* key sources of error for the snow density profile.

Snow settling. Metamorphism of snow crystals towards rounded grains is the primary reason for snow settling of fresh snow. The model accounts for this settling with the term CR_{metam} , which is given as a function of air temperature, snow density and liquid water content (Equations 11 and 12). To illustrate the sensitivity of the snowpack layering on CR_{metam} we ran two simulations, in which the parameters c_2 , c_3 and c_4 (Equation 11) were changed by 50% so that enhanced ‘metamorphism settling’ was created in one case, whereas reduced ‘metamorphism settling’ was simulated in the other case.

Similar to the previous sensitivity tests, the simulations showed that the altered ‘metamorphism settling’ rate was not able to generate additional distinct snow layers either (Figure 10). Of course, enhanced ‘metamorphism settling’ led to an overall increase in snow density, but it did not intensify the contrasts between layers. We concluded that the term CR_{metam} did not influence the layering of this subalpine snowpack more than marginally.

Water flow velocity in the snowpack. The velocity of the water redistribution from layer to layer has an impact on the water and ice content of the single layers, and hence on the density. We investigated how much the snow density profile responded to the water flow velocity by decreasing the saturated hydraulic permeability of the snow. In the model, k_{sat} is a function of snow density and grain diameter (Equation 19). We altered k_{s1} from 0.077 to 0.01 and later to 0.001 while keeping the density dependence (k_{s2}) unchanged, following the experiments of Shimizu (1970).

The decreased water redistribution in the snow did not change the total snow depth significantly, and the water equivalent of the total snowpack also remained unchanged for most of the winter season. On the other hand, we noticed an effect on the snowpack layering owing to increased refreezing of liquid water. As shown in Figure 11 for two selected dates (13 February, just after a minor snowmelt event in February; 30 March,

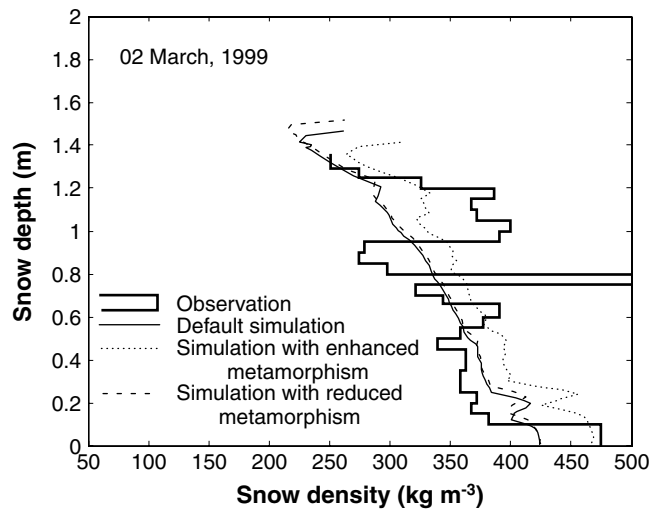


Figure 10. Sensitivity test of the parameters related to metamorphism (Equation 11): simulated and observed snow density profiles for a day shortly after the main snowfall of February 1999

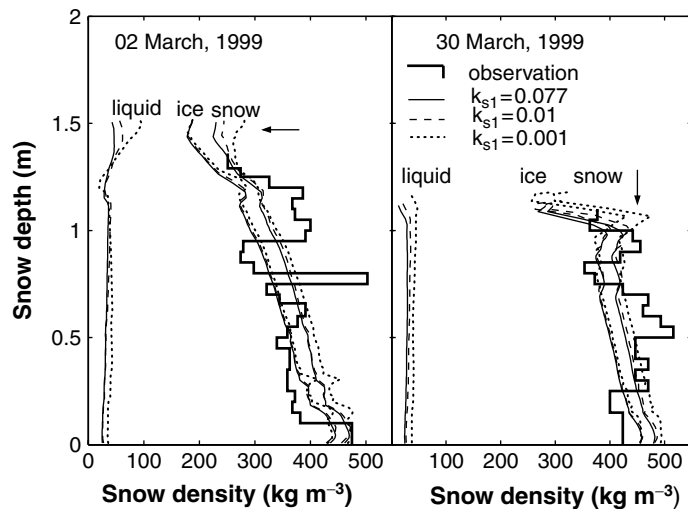


Figure 11. Sensitivity test of the saturated hydraulic conductivity function (k_{s1} in Equation 19): Simulated and observed snow density profiles for two dates in winter 1998–99

during the first major ablation period), layers of high density were somewhat more pronounced when the hydraulic conductivity was reduced. For example, the infiltration of liquid water was reduced at the top of the snowpack on 2 March, and as a result a layer of higher density was simulated at the top of the snowpack on 30 March, which was in agreement with our field observation. On the other hand, compared with the default simulation no additional distinct layers formed and the density was still out by about 20% for the dense layer at $z = 0.5$ to 0.6 m.

The density spike at $c. 0.8$ m is probably due to liquid water. This is supported by manual observation of increased wetness and explains why this spike is not visible in the respective translucent snow profile (Bohren and Barkström, 1974).

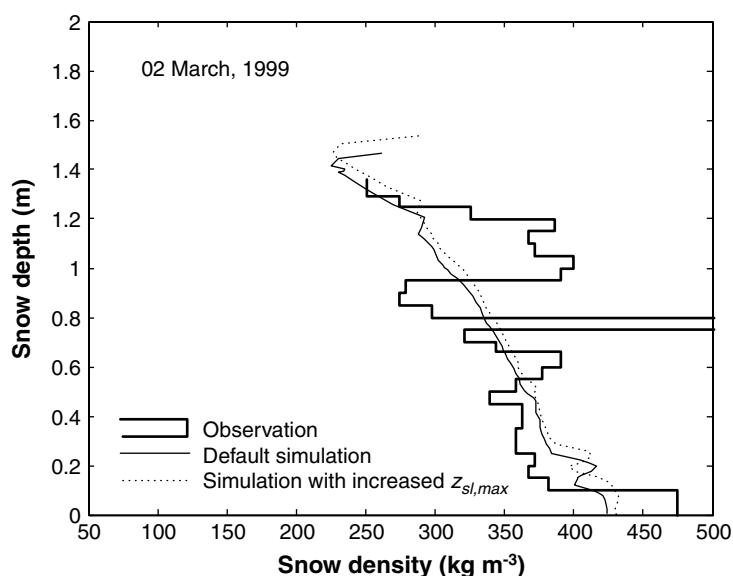


Figure 12. Sensitivity test of the maximum layer thickness: simulated and observed snow density profiles for a day shortly after the main snowfall of February 1999

Maximum layer thickness. The limitation of the layer thickness during snowfall may cause single layers to settle to some few millimetres only, owing to metamorphism and overburden pressure. When layers settle below a given minimum layer thickness ($z_{sl,min} = 0.005$ m) adjacent layers merge, which leads to a smoothing of the density gradient. Thus, we suspected that the choice of the maximum layer thickness would have had a non-negligible impact on the snow density profile. This hypothesis was tested by increasing the layer maxima to $z_{sl,max,top} = 0.05$ m, $z_{sl,max,second} = 0.08$ m and $z_{sl,max,general} = 0.1$ m. This did not enhance the snow layering significantly. Figure 12 shows that the density profile on 2 March, i.e. shortly after the main snow accumulation, was almost identical for the default simulation and the simulation with increased $z_{sl,max}$. Only a minor difference in snow depth resulted from thicker snow layers.

Snow grain growth. In the model, the snow grain size has a major influence on the water flow velocity that controls the liquid water redistribution in the snowpack (Equation 19), and hence an indirect effect on the snow density. To test the sensitivity of the snow grain growth parameterization we increased and decreased, respectively, the two parameters determining the grain growth rate, g_1 and g_2 (Equation 14), by 50%.

A considerable increase and decrease, respectively, of the grain size in the entire profile resulted from these changes. However, a more distinct layering with respect to grain size was not achieved and the simulation of snow depth and density was not influenced significantly (Figure 13).

Microstructure and viscosity. In the SNTHERM model, the compaction of snow layers is a function of T_{Snow} , γ_{ice} , γ_{liq} , only (Equations 9–13). However, it is plausible that the microstructure of the snow significantly configures its mechanical properties, i.e. the viscosity. To highlight the importance of accounting for effects of microstructure on compaction when simulating formation of distinct layers we compared SNTHERM with the SNOWPACK model (Lehning *et al.*, 1998, 1999).

In contrast to SNTHERM, the SNOWPACK model calculates snow settling as a function of the stress normal to the slope and the elastic and viscous strain (Bartelt and Lehning, 2002; Lehning *et al.*, 2002a, b). Further, in SNOWPACK, liquid water is transported downwards to the next layer when the liquid water content exceeds $0.025 \text{ m}^3 \text{ m}^{-3}$.

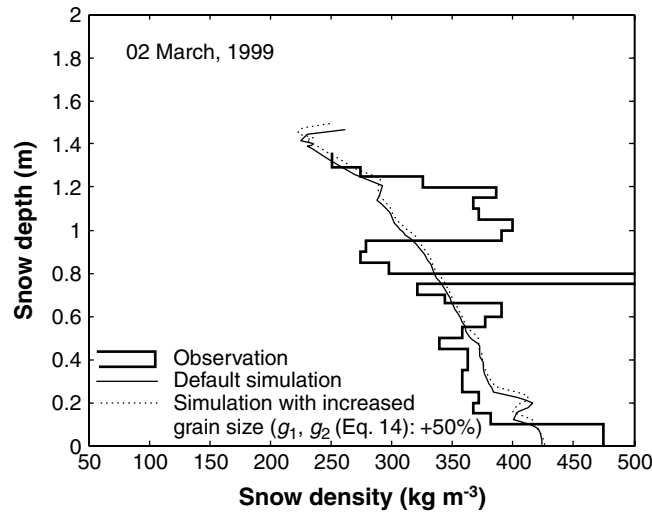


Figure 13. Sensitivity test of the grain size functions (Equation 14) (bottom): simulated and observed snow density profiles for a day shortly after the main snowfall of February 1999

Using the parameterization of Lehning *et al.* (2002b), the SNOWPACK model simulated the snow water equivalent and depth with a similar agreement to that of SNTHERM (not shown in a graph). The SNOWPACK model overestimated the density of the upper layers, probably owing to too high new-snow densities or compaction rates for fresh snow (Figure 14).

The density profiles of SNOWPACK did not show many more layers than SNTHERM. Furthermore, the additional layer at $z = 0.3$ to 0.5 m on 13 February is not contained in the measurement. Much of the density

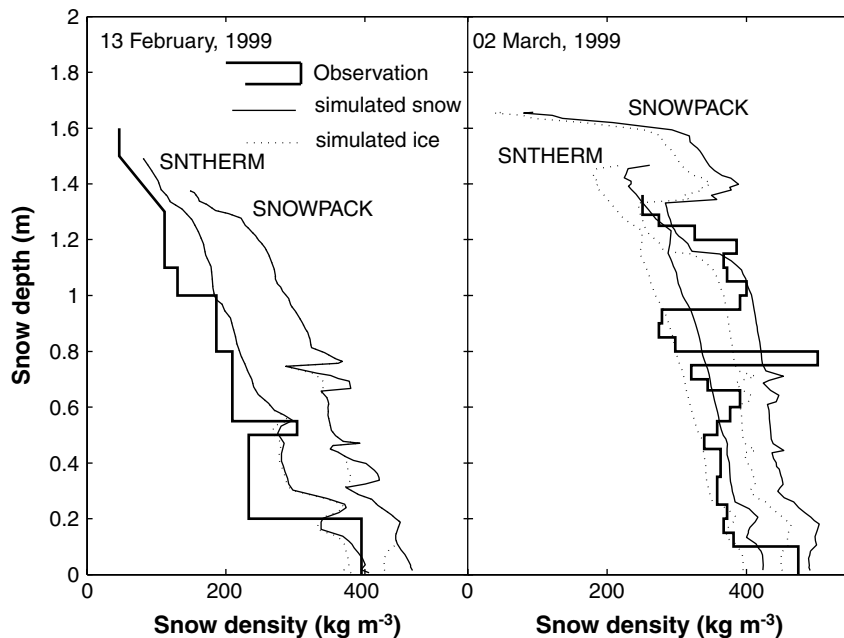


Figure 14. Comparison of SNTHERM and SNOWPACK: simulated and observed snow density profiles for two dates in winter 1999

increase of this layer is due to liquid water produced before 7 February, which infiltrated to this depth in the SNOWPACK simulation.

In the SNOWPACK simulation, however, the layers were more pronounced and persistent than in the SNATHERM model. This is clearly visible for the layer densified by surface melt in January, which was at $z = 0.55$ on 13 February and at $z = 0.5$ on 2 March. Neither models reproduced the dense layer at $z = 0.8$ m on 2 March, which was related to increased liquid water content. Boundaries between a fine-textured layer above a coarse-textured layer have been found to act as capillary barrier (Jordan, 1995; Waldner *et al.*, 2004). However, the microstructural parameters simulated by SNOWPACK met the conditions for a capillary barrier at this height (Marsh and Woo, 1984). Furthermore, preferential flow is likely to be triggered at such barriers owing to hydraulic instabilities (Waldner *et al.*, 2004) and influences water transport and content.

DISCUSSION AND CONCLUSIONS

As a general conclusion from the comparison of the snowpack model presented here with the snow measurements at the subalpine site at Erlenhöhe during winter 1998–99, we can state that, on the one hand, the model succeeded very well in reproducing the ‘bulk properties’ (snow depth, snow water equivalent, average snow density and general trend in the vertical snow density profile) of this snowpack, as well as variables related to the surface energy balance (net radiation) and heat transport (temperatures in the snowpack). On the other hand, the model was not able to simulate satisfactorily the strongly layered nature of the subalpine snowpack.

The sensitivity analysis showed us that model uncertainties related to the surface energy balance were probably not the major reason. For several components we received an impression of the uncertainty of the surface energy balance during validation with $R_{S\uparrow}$, $R_{L\downarrow}$ (Figure 4). Although we are aware of the key importance of the surface energy balance for the formation of new snow layers (Lehning *et al.*, 2001), the study nevertheless demonstrated that the accuracy of our radiation balance is high enough in relation to the relatively low sensitivity of the snow layer pattern on, for example, snow albedo or roughness length. However, there might be processes related to the snow surface energy balance not treated explicitly by the model that might be important for the formation of distinct snow layers.

A more important reason for the inability of the model to produce the true snow layer structure seems to be related to the water flow in the snowpack and the compaction of layers. The model approach in SNATHERM is based on studies in ‘homogeneous’ snow and does not explicitly account for the snow microstructure and the shape of the snow particles. Such an approach is of only limited use when applied to a field profile with distinct layers.

The comparison with SNOWPACK (Figure 14) showed that the model’s inability to reproduce can be explained partly by effects of the snow microstructure on its viscosity and elasticity, which are not included in the SNATHERM model.

The sensitivity analyses showed that the layer pattern of the subalpine snowpack is sensitive to the hydraulic conductivity, and hence to the flow rate. In natural conditions, the hydraulic conductivity, similar to the compaction, is influenced by the snow microstructure.

A further constraint for the reproduction of the layering is that the model accounts neither for the capillary barrier effect between a fine-textured layer above a coarse-textured layer (Jordan, 1995; Waldner *et al.*, 2004; Coléou *et al.*, 1999; Jordan *et al.*, 1999) nor for preferential flow within the pack. A capillary barrier not only slows down the vertical flux, it also forms ice layers (when refreezing occurs) and induces lateral water flow. Furthermore, capillary barriers influence the snow density and microstructure through the feedback mechanism between liquid water content and snow metamorphism. Preferential flow directly influences liquid water content and distribution within a snow pack.

With the uncertainties with regard to the absolute values and spatial variation of the hydraulic conductivity in mind, as well as the limitation with regard to the (one-dimensional) model approach, it seems likely that the mismatch of the snow layering is related to the water redistribution in the snowpack.

Our sensitivity analysis showed that the snow layer pattern was not significantly influenced by the choice of the minimum or maximum thickness for a layer. Maybe the key question is rather *how* layers are merged, i.e. with which strategy. In the present version, thin layers are always combined with the thinnest neighbour, but a better way would be to avoid mixing layers from different snow fall events and to combine the layers with the closest density as already implemented in the CROCUS model (Brun *et al.*, 1989).

ACKNOWLEDGEMENTS

The authors would like to thank a number of people who contributed with valuable assistance and comments to this paper: Charles Fierz, Felix Forster, Bruno Fritsch, Per-Erik Jansson, Michael Lehning, Martin Schneebeli and Hans Wunderli. This work was funded by the Royal Institute of Technology, Stockholm, the Swedish Research Council (Grant No. 629-2002-724), and the Swiss National Science Foundation (Grant No. 2100-52352.97).

REFERENCES

- Ångström A. 1924. Solar and terrestrial radiation. *Quarterly Journal of the Royal Meteorological Society* **50**: 121–125.
- Bartelt P, Lehning M. 2002. A physical SNOWPACK model for the Swiss avalanche warning Part I: numerical model. *Cold Regions Science and Technology* **35**: 123–145.
- Bohren CF, Barkström B. 1974. Theory of optical-properties of snow. *Journal of Geophysical Research* **79**: 4527–4535.
- Brun E, Martin E, Simon V, Gendre C, Coléou C. 1989. An energy and mass model of snow cover suitable for operational avalanche forecasting. *Journal of Glaciology* **35**: 333–342.
- Brun E, David P, Sudul M, Brunot G. 1992. A numerical-model to simulate snow-cover stratigraphy for operational avalanche forecasting. *Journal of Glaciology* **38**: 13–22.
- Colbeck SC, Akitaya E, Armstrong R, Gubler H, Lafeuille J, Lied K, McClung D, Morris E. 1990. *The International Classification for Seasonal Snow on the Ground*. International Commission on Snow and Ice of the International Association of Scientific Hydrology: Wallingford; 23.
- Coléou C, Xu K, Lesaffre B, Brzoska JB. 1999. Capillary rise in snow. *Hydrological Processes* **13**: 1721–1732.
- Durand Y, Giraud G, Brun V, Merindol L, Martin E. 1999. A computer-based system simulating snowpack structures as a tool for regional avalanche forecasting. *Journal of Glaciology* **45**: 469–484.
- Gustafsson D, Stähli M, Jansson P-E. 2001. The surface energy balance of a snow cover: comparing measurements to two different simulation models. *Theoretical and Applied Climatology* **70**: 81–96.
- Hardy JP, Davis RE, Jordan R, Ni W, Woodcock CE. 1998. Snow ablation modelling in a mature aspen stand of the boreal forest. *Hydrological Processes* **12**: 1763–1778.
- Hedstrom NR, Pomeroy JW. 1998. Measurement and modeling of snow interception in the boreal forest. *Hydrological Processes* **12**: 1611–1625.
- Jansson P-E, Moon D. 2001. A coupled model of water, heat and mass transfer using object orientation to improve flexibility and functionality. *Environmental Modeling and Software* **16**: 37–46.
- Johnsson H, Jansson P-E. 1991. Water-balance and soil-moisture dynamics of field plots with barley and grass ley. *Journal of Hydrology* **129**: 149–173.
- Jordan R. 1991. *A One-dimensional Temperature Model for Snow Cover*. Special Report 91-16, U.S. Army Corps of Engineers, Cold Regions Research and Engineering Laboratory; Manover, NH; 49.
- Jordan R. 1995. Effects of capillary discontinuities on water-flow and water-retention in layered snow covers. *Defence Science Journal* **45**: 79–91.
- Jordan R. 1996. *User's guide for USACRREL one dimensional snow temperature model (SN THERM 89)*. U.S. Army Corps of Engineers, Cold Regions Research and Engineering Laboratory; Manover, NH; 18.
- Jordan RE, Andreas EL. 1999. Heat budget of snow-covered sea ice at North Pole 4. *Journal of Geophysical Research* **104**: 7785–7806.
- Jordan RE, Hardy JP, Perron FE, Fisk J, Fisk DJ. 1999. Air permeability and capillary rise as measures of the pore structure of snow. *Hydrological Processes* **13**: 1721–1732.
- Keller HM, Forster F. 1991. Simulating soil moisture and runoff components to estimate variability of streamflow chemistry. *International Association of Hydrological Sciences Publication* **202**: 143–151.
- Koivusalo H, Heikinheimo M, Karvonem T. 2001. Test of a simple two-layer parameterisation to simulate the energy balance and temperature of a snow pack. *Theoretical and Applied Climatology* **70**: 65–79.
- Konzelmann T, Vandewal RSW, Greuell W, Bintanja R, Henneken EAC, Abeouchi A. 1994. Parameterization of global and long wave incoming radiation for the Greenland ice-sheet. *Global and Planetary Change* **9**: 143–164.

- Lehning M, Bartelt P, Brown RL. 1998. The mass and energy balance of the SNOWPACK model. *EOS, Transactions, American Geophysical Union, Fall Meeting, Supplement* **79**: F272.
- Lehning M, Bartelt P, Brown B, Russi T, Stöckli U, Zimmerli M. 1999. SNOWPACK model calculations for avalanche warning based upon a new network of weather and snow stations. *Cold Regions Science and Technology* **30**: 145–157.
- Lehning M, Bartelt P, Brown B, Fierz C. 2002a. A physical SNOWPACK model for the Swiss avalanche warning Part III: meteorological forcing, thin layer formation and evaluation. *Cold Regions Science and Technology* **35**: 169–184.
- Lehning M, Bartelt P, Brown B, Fierz C, Satyawali P. 2002b. A physical SNOWPACK model for the Swiss avalanche warning Part II: snow microstructure. *Cold Regions Science and Technology* **35**: 147–167.
- Lehning M, Fierz C, Lundy C. 2001. An objective snow profile comparison method and its application to SNOWPACK. *Cold Regions Science and Technology* **33**: 253–261.
- Marsh P, Woo M-K. 1984. Wetting front advance and freezing of meltwater within a snow cover: 1. Observations in the Canadian Arctic. *Water Resources Research* **20**: 1853–1864.
- Plüss C, Mazzoni R. 1994. The role of turbulent heat fluxes in the energy balance of the high alpine snow cover. *Nordic Hydrology* **25**: 25–38.
- Rowe CM, Kuivinen KC, Jordan RE. 1995. Simulation of summer snowmelt on the Greenland ice sheet using a one-dimensional model. *Journal of Geophysical Research* **100**: 16 265–16 273.
- Shimizu H. 1970. Air permeability of deposited snow. *Low Temperature Sciences Series A* **22**: 1–32.
- Stähli M, Jansson P-E, Lundin L-C. 1999. Soil moisture redistribution and infiltration in frozen sandy soils. *Water Resources Research* **35**: 95–103.
- Stähli M, Papritz A, Waldner P, Forster F. 2000. Die Schneedeckenverteilung im voralpinen Einzugsgebiet Erlenbach während des Rekordwinters 1998/99. *Schweizerische Zeitschrift für Forstwesen, Swiss Forestry Journal* **151**: 192–197.
- Waldner P, Schneebeli M, Wunderli H. 2000. Nitrate release from a melting snow pack in Alptal (Canton of Schwyz, Switzerland). *Swiss Forestry Journal* **151**: 198–204.
- Waldner P, Schneebeli M, Zimmermann U, Flüeler H. 2004. Effect of snow structure on water flow and solute transport. *Hydrological Processes* **18**: 1271–1290.
- Wiesmann A, Mätzler C. 1999. Microwave emission model of layered snowpacks. *Remote Sensing of Environment* **70**: 307–316.